Absolute total and partial cross sections for the electron impact ionization of diborane (B_2H_6)

R. Basner[a] and M. Schmidt
Institut für Niedertemperatur-Plasmaphysik, Friedrich-Ludwig-Jahn-Strasse 19, D-17489 Greifswald, Germany

K. Becker
Department of Physics and Engineering Physics, Stevens Institute of Technology, Hoboken, New Jersey 07030

(Received 20 September 2002; accepted 6 November 2002)

We measured absolute partial cross sections for the formation of all singly charged positive ions formed by electron impact on diborane (B_2H_6) from threshold to 200 eV using a time-of-flight mass spectrometer. The absolute total ionization cross section of B_2H_6 was obtained as the sum of all measured partial ionization cross sections. Dissociative ionization resulting in thirteen different fragment ions was found to be the dominant ionization process, although we found evidence of the presence of the $B_2H_6^+$ parent ion. The ion spectrum at all impact energies including in the energy region below 40 eV, which is of special interest for low-temperature plasma technology, is dominated by $B_2H_5^+$, $B_2H_4^+$, and $B_2H_2^+$ fragment ions. The $B_2H_5^+$ fragment ion has the largest partial ionization cross section with a maximum value of 2.87×10^{-16} cm^2 at 60 eV. We also observed H^+, H_2^+, and H_3^+ fragment ions, but no ion signals were found that can be attributed to the formation of doubly charged ions. Additional measurements using a sector-field mass spectrometer revealed that all fragment ions containing one boron atom (B^+, BH_y^+, $y=1-3$) and H^+ are formed with significant excess kinetic energy. The mass spectrum of ions formed by electron impact on B_2H_6 at 70 eV in our experiments revealed distinctly larger abundances of the fragment ions BH_3^+, BH_2^+, and BH^+ than earlier mass spectrometric measurements. © *2003 American Institute of Physics.* [DOI: 10.1063/1.1533013]

I. INTRODUCTION

Plasma-enhanced chemical vapor deposition processes are an important area of application of nonthermal, low-pressure plasmas. In these plasmas direct and/or dissociative electron impact ionization of the neutral heavy particles in the ground or in excited states is an important initial and in many plasmas the dominant ion and radical formation process depending on the shape of the electron energy distribution function. Diborane, B_2H_6, is used as a precursor for the deposition of cubic boron nitride (BN) films of high bardness and high chemical resistance using B_2H_6-plasmas with admixtures of H_2-NH_3 and $N_2-He-Ar$.[1,2] Furthermore, doping of silicon with boron for applications in semiconductor devices is successfully achieved by different plasma-enhanced methods in diborane containing gas mixtures.[3–5] Quantitative knowledge of electron impact cross sections of diborane for excitation, dissociation, and ionization, is necessary for the understanding and optimization of the plasma processes.

Earlier work on dissociative ionization of diborane includes mass spectrometric measurements of relative intensities for fragmentation, pyrolysis, and the determination of appearance energies.[6–10] Appearance energies of the fragment ions were also studied by photoelectron spectroscopy.[11–15] The mass spectrum of diborane can be found in standard mass spectral compilations.[16]

This paper reports the results of a quantitative, mass spectrometric study of the electron impact ionization of B_2H_6 from threshold to 200 eV. The absolute partial cross sections were determined of the fragment ions $B_2H_x^+(x=1-6)$, B_2^+, $BH_y^+(y=1-3)$, B^+, and $H_z^+(z=1-3)$. The total ionization cross section was obtained as the sum of the measured partial cross sections. These measurements continue our ongoing study of ionization cross-section measurements of molecules, which are important for a microscopic understanding of the processes in low-temperature processing plasmas.[17–24] Preliminary results of this study have already been presented at a conference.[25]

II. EXPERIMENTAL APPARATUS

The measurements were carried out using a time-of-flight mass spectrometer (TOF-MS) that is shown schematically in Fig. 1 and that has been described in detail elsewhere.[22–24] The TOF-MS can be operated either in a linear mode using detector I or in a reflection mode using the reflector (grids: G_3, G_4, G_5) and detector II. In the present study, all measurements were performed with the TOF-MS operated in the linear mode to ensure complete ion transport from the ion source to the detector. Diborane was stored in a stainless steel reservoir at room temperature at a pressure of 100 Pa. The ion source chamber was filled with a well-defined B_2H_6/Ar mixture through precision leak valves up to partial pressures of about 1×10^{-4} Pa in an effort to facilitate

[a]Electronic mail: basner@inp-greifswald.de

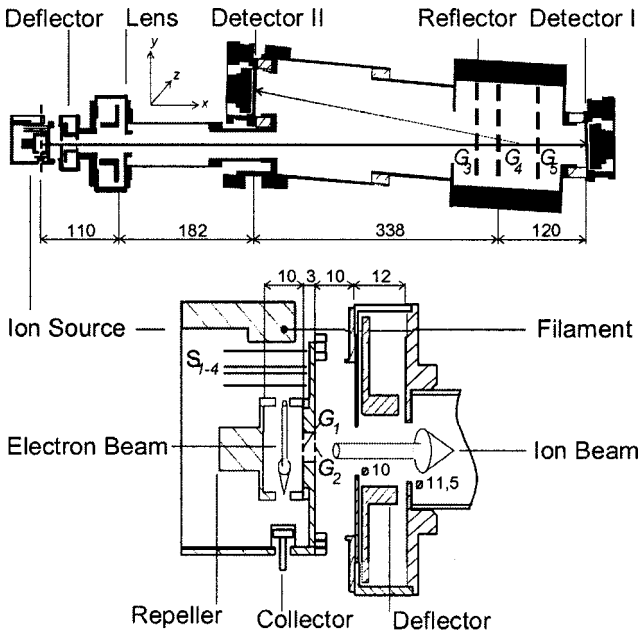

FIG. 1. Schematic diagram of the time-of-flight mass spectrometer and a detailed view of the electron impact ion source used in the present study (all dimensions are in mm).

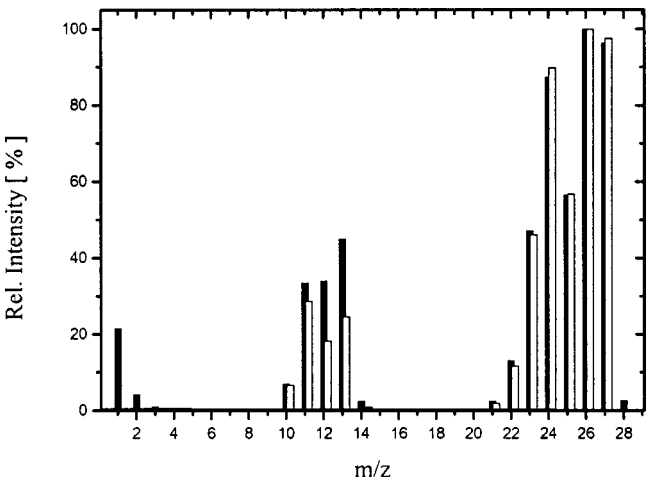

FIG. 2. Mass spectrum of B_2H_6 at 70 eV impact energy measured with the time-of-flight mass spectrometer in the linear mode (filled bars) in comparison with the reference mass spectrum (open bars)—Ref. 16.

the simultaneous measurements of the ions from diborane and Ar under identical operating conditions. The relative partial diborane ionization cross sections were put on an absolute scale by normalization relative to the total Ar ionization cross section of 2.77×10^{-16} cm^2 at 70 eV[26] which was recently confirmed with a lower error margin of 5%.[27] Taking into account the uncertainties of $\pm5\%$ in the Ar reference cross section,[26,27] the statistical uncertainty in our pressure measurement of $\pm3\%$ and an uncertainty of typically 3%–12% resulting from the counting statistics and the deconvolution of the various isotope components from the measured ion signals, we assign an overall uncertainty of not more than $\pm20\%$ to the absolute ionization cross sections reported here except in the case of B_2H^+ with an uncertainty of $\pm24\%$ (see the following discussion).

Typically, the electron gun was operated using electron pulses of 90 ns width at a repetition rate of 15 kHz. The electron beam had a diameter of about 0.6 mm in the interaction region and the amplitude of the electron pulse was in the range from 1 to 10 μA with energy spread of about 0.5 eV (full width at half-maximum). The impact energy was varied from 5 to 200 eV and the electron beam was guided by a weak magnetic field (200 G). A voltage of 1 kV (extraction fields of 1 kV cm^{-1}) was applied to the repeller roughly 10 ns after the incident electron pulse passed through the ionization region. This extraction pulse accelerates the ions formed by electron impact toward the grounded ion source exit aperture and the entrance electrode of the flight tube using a -2.8 kV bias voltage. We maintained operating conditions under which 100% ion transmission of all ions from the ion source to the detector was established with the exception of ion loss at the grids G_1 and G_2. The detector arrangement (detector I) is placed at the end of the flight tube. The output from the MCP is preamplified and recorded with a 2 GHz multiscaler (FAST ComTec, Model 7886) with a time resolution of 500 ps. Our TOF-MS was operated in such a way that no more than one ion was created during each electron pulse. This resulted in low overall count rates and comparatively long data acquisition times, but ensured, on the other hand, that dead time corrections to the recorded signal rates were negligible (see Refs. 22–24 for more details).

B_2H_6 with two hydrogen bridges connecting the two BH_2 groups and with no direct B–B chemical bond is known to be unstable even at room temperature.[28] The decomposition of the molecule follows a complex decay route via unstable intermediate species and leads to B_4H_{10}, B_5H_{11}, and H_2 as first stable decomposition products. We observed the thermal decomposition of B_2H_6 in our reservoir through traces of B_4H_{20} and B_5H_{11} that were identified by the mass spectrum,[16] albeit with low intensities of less than 1% of the intensity of parent $B_2H_6^+$ ion peak. However, we did observe an intense H_2^+ ion signal, which increased with the residence time of the B_2H_6 in the storage reservoir. The main contribution of this signal was identified as arising from the direct ionization of the H_2 that was produced in the decomposition of B_2H_6 in the storage reservoir. Only a small fraction of the H_2^+ signal was attributable to H_2^+ fragment ions formed by dissociative ionization of B_2H_6. The H_2 resulting from the decomposition of B_2H_6 in the reservoir was routinely removed by repeatedly freezing the B_2H_6 and pumping out the reservoir. This procedure produced a target sample that was sufficiently free of H_2 contamination for about 1 h, at which point the purification of the sample has to be repeated.

III. RESULTS AND DISCUSSIONS

The mass spectrum of B_2H_6 at an electron energy of 70 eV derived from measurements carried out with the TOF-MS operated in the linear mode is shown in Fig. 2 and the result is compared to the mass spectrum of B_2H_6 found in the NIST database.[16] In both spectra the isotopic composition of the target, i.e., contributions from ^{10}B and ^{11}B at a ratio of 0.19:0.81[29] were not resolved. Our results are in excellent

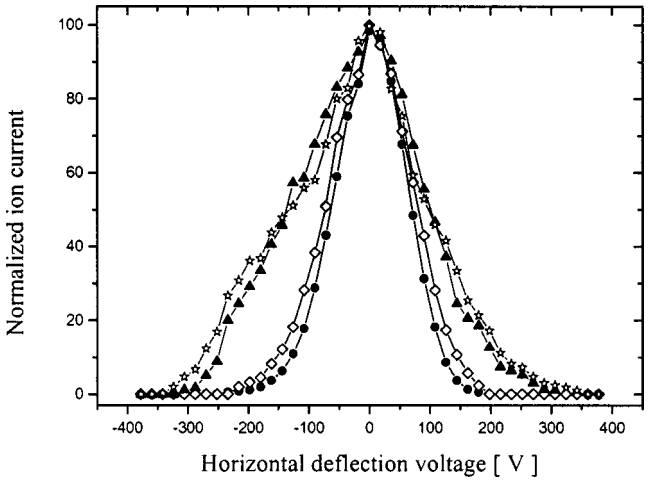

FIG. 3. Normalized ion beam currents of the ions at m/z 40, Ar^+ (closed circles) at m/z 24, a mixture of 4% $^{10}B_2H_4^+$, 14% $^{10}B^{11}BH_3^+$, and 82% $^{11}B_2H_2^+$ (open diamonds) at m/z 12, a mixture of 32% $^{10}BH_2^+$ and 68% $^{11}BH^+$ (closed triangles) and at m/z 1, H^+ (open stars) as a function of the horizontal deflection voltage at 70 eV impact energy. These data were obtained with a double-focusing sector-field mass spectrometer using a modified ion extraction stage (Refs. 20–22).

agreement with the NIST data for the heavier ions, but noteworthy differences are apparent for ions of lower mass. The intensities of the ions BH_3^+, BH_2^+, and BH^- are distinctly higher in our spectrum than the corresponding intensities found in the NIST database.[16] The reason for this discrepancy may be a higher detection efficiency of our TOF-MS for ions, which are formed with significant amounts of excess kinetic energy. We carried out qualitative determinations of the excess kinetic energy for all fragment ions by performing a full horizontal sweep of the extracted ion beam using a double-focusing mass spectrometer.[20–22] The results of these measurements are presented in Fig. 3. The shape of the Ar^+ ion signal is characteristic of a beam of ions without excess kinetic energy. The shape of the ion signal at *m/z* 24 (a mixture of 4% $^{10}B_2H_4^+$, 14% $^{10}B^{11}BH_3^+$, and 82% $^{11}B_2H_2^+$) is representative for the H_2^+ ion and all fragment ions of B_2H_6 containing two B atoms. The curve shows some broadening which is indicative of a small amount of excess kinetic energy. All other ions show beam profiles that suggest a broad distribution of excess kinetic energies as shown for m/z 12 (a mixture of 32% $^{10}BH_2^+$ and 68% $^{11}BH^+$) and m/z 1, the H^+ fragment ion in Fig. 3. We also found measurable ion signals for the ion H_3^+. No appreciable ion signals solely attributable to the formation of certain doubly-charged ions were detected as evidenced by the absence of any peaks in the recorded mass spectrum at m/z values of 10.5, 11.5, 12.5, and 13.5 (see Fig. 2). The absence of any discernible ion peaks at these m/z values in several measurements where the TOF-MS was operated in the reflection mode with higher mass resolution confirms this result. Thus, we are confident that the cross sections leading to the formation of doubly charged ions from B_2H_6 are at least 2 orders of magnitude smaller than even the cross sections for the formation of those singly charged ions formed with low probability.

Because the mass resolution of the TOF-MS is not sufficient to resolve the signals attributable to the two isotopes of B, we measured the ion efficiency curves corresponding to all ions that contribute to a given mass number. Using the known abundances of ^{10}B and ^{11}B (0.19 and 0.81[29]) and the measured intensity of the uncontaminated ion peak at m/z 14 ($^{11}BH_3^+$), we then calculated successively the contribution of each ion to m/z 13, 12, and 11 for every value of electron impact energy. A similar procedure was applied to all mass numbers from 21 to 28 by solving a system of linear equations resulting from the binominal intensity distribution of the isotope contributions of $^{10}B_2$: $^{10}B^{11}B$:$^{11}B_2$ = 6.17:49.69:100.[30] The calculation started with the measured intensity of $^{11}B_2H_6^+$ at m/z 28 and resulted in the three separate isotopic contributions for each ion at all electron impact energies. The deconvolution of the ion signals that contain contributions from more than one ion due to the two B isotopes into isotopically resolved ion signals was carried out with data with a standard deviation of 2%–5%. The only exception to this is the ion signal at m/z 20 ($^{10}B_2^+$) with 12% standard deviation. As a consequence, the application of the error propagation law in the deconvolution procedure (when we start from the uncontaminated ion peak with the highest m/z value in each group) leads to uncertainties in the resulting isotopically pure ion signals of less than $\pm 8\%$ except in the cases of B_2^+ (12%) and the B_2H^+ ion signal where the error propagation leads to a $\pm 16\%$ error margin.

The partial ionization cross sections for the ions were then obtained by adding the isotopic contributions. The numerical values of the partial ionization cross sections and the total ionization cross section (the sum of all partial cross sections) as a function of the energy of the ionizing electrons from threshold to 200 eV are given in Table I. The corresponding cross-section curves are shown in Figs. 4 and 5.

The measured appearance energies for the various ions with their respective uncertainties are given in the last line of Table I. The appearance energies were obtained from a linear extrapolation of the measured ion efficiency curve near threshold for all mass numbers without isotopic interferences. In the case of an ion mixture, the separation of the isotopic contributions was done as described before. Our appearance energy values are in agreement with previously reported electron impact data as well as with photoionization data (see Ref. 16) with the exception of the fragment ions $BH_x^+ (x=1-3)$, for which we obtained somewhat higher appearance energy values. It is noteworthy that we observed extended curvatures in the near-threshold regions for the light fragment ions, which significantly exceeded the curvature in the threshold region that is attributable to the energy spread in the electron beam. In almost all cases, this extended curvature was responsible for the quoted uncertainty in the respective appearance energy determination. We attribute this curvature primarily to the generation of fragment ions with broad distributions of excess kinetic energy (see Fig. 3). Reference data for the appearance energy of H^+, H_2^+, and H_3^+ from B_2H_6 are not available. The formation process leading to H_3^+ fragment ions could not be uniquely identified. While it is well known that stable H_3^+ ions are formed in gas discharges by ion molecule reactions, e.g., between H_2^+ and H_2 with large rate constants,[31,32] the formation of these ions has not been observed in the dissociative electron impact

TABLE I. Absolute partial and total electron impact ionization cross sections for B_2H_6 as a function of electron energy from threshold to 200 eV and measured appearance energies (AE) of the respective ions (last line).

	Ionization cross section (10^{-16} cm^{-2})						
Electron energy (eV)	H^+	H_2^+	H_3^+	B^+	BH^+	BH_2^+	BH_3^+
12							
12.5							
13							
13.5							
14							
14.5							
15							
15.5							
16							
16.5		0.002					0.001
17		0.004				0.007	0.002
17.5		0.006				0.012	0.003
18		0.008				0.019	0.003
18.5		0.01				0.025	0.004
19		0.011				0.033	0.004
19.5		0.013			0.002	0.041	0.005
20		0.014		0.009	0.004	0.05	0.006
21		0.017		0.028	0.008	0.069	0.007
22		0.019		0.047	0.013	0.091	0.008
23		0.021		0.066	0.019	0.125	0.009
24		0.023		0.087	0.024	0.162	0.01
25		0.025		0.11	0.03	0.211	0.011
26		0.027		0.14	0.04	0.243	0.012
28		0.032		0.199	0.056	0.311	0.014
30		0.036		0.266	0.082	0.408	0.016
32	0.031	0.04		0.321	0.109	0.471	0.018
36	0.079	0.048		0.421	0.183	0.604	0.025
38	0.109	0.052	0.002	0.462	0.224	0.676	0.029
42	0.165	0.059	0.006	0.527	0.304	0.794	0.038
46	0.218	0.063	0.009	0.575	0.357	0.86	0.048
50	0.269	0.067	0.012	0.611	0.409	0.926	0.055
55	0.326	0.071	0.015	0.633	0.46	0.997	0.058
60	0.364	0.075	0.017	0.647	0.506	1.03	0.06
65	0.399	0.078	0.019	0.659	0.534	1.05	0.061
70	0.416	0.08	0.02	0.672	0.554	1.07	0.06
75	0.429	0.082	0.021	0.68	0.568	1.08	0.059
80	0.437	0.083	0.022	0.679	0.576	1.08	0.058
90	0.444	0.082	0.022	0.654	0.569	1.04	0.056
100	0.438	0.08	0.02	0.603	0.545	1.01	0.054
110	0.416	0.077	0.019	0.578	0.514	0.975	0.052
120	0.389	0.074	0.018	0.552	0.493	0.943	0.051
140	0.313	0.067	0.016	0.522	0.445	0.89	0.049
160	0.252	0.059	0.015	0.483	0.403	0.84	0.047
180	0.213	0.052	0.014	0.468	0.361	0.784	0.046
200	0.181	0.046	0.013	0.453	0.334	0.732	0.045
AE (eV)	30.0±2.5	16.0±1.4	36.0±3.5	19.4±1.4	19.0±2.3	16.6±2.1	15.1±1.6

	B_2^+	B_2H^+	$B_2H_2^+$	$B_2H_3^+$	$B_2H_4^+$	$B_2H_5^+$	$B_2H_6^+$	Total
12						0.068	0.002	0.07
12.5					0.038	0.146	0.004	0.188
13					0.075	0.25	0.006	0.331
13.5					0.14	0.36	0.009	0.509
14					0.22	0.5	0.011	0.731
14.5			0.055	0.019	0.29	0.6	0.013	0.977
15			0.13	0.031	0.35	0.73	0.014	1.255
15.5			0.2	0.051	0.42	0.91	0.016	1.597
16			0.29	0.079	0.49	1.03	0.017	1.906
16.5			0.36	0.105	0.57	1.14	0.018	2.196
17			0.46	0.128	0.65	1.3	0.019	2.57
17.5			0.57	0.158	0.73	1.46	0.02	2.959
18			0.67	0.187	0.8	1.58	0.021	3.288

TABLE I. (*Continued.*)

Electron energy (eV)	Ionization cross section (10^{-16} cm^{-2})							
	B_2^+	B_2H^+	$B_2H_2^+$	$B_2H_3^+$	$B_2H_4^+$	$B_2H_5^+$	$B_2H_6^+$	Total
18.5			0.77	0.222	0.87	1.66	0.022	3.583
19			0.85	0.26	0.93	1.74	0.024	3.852
19.5			0.95	0.317	0.99	1.84	0.025	4.183
20			1.06	0.392	1.05	1.92	0.026	4.531
21			1.19	0.466	1.11	2.06	0.028	4.983
22		0.017	1.33	0.545	1.17	2.19	0.03	5.46
23		0.0374	1.46	0.601	1.22	2.27	0.032	5.857
24		0.048	1.58	0.649	1.26	2.36	0.034	6.237
25	0.003	0.066	1.69	0.677	1.3	2.41	0.036	6.569
26	0.007	0.081	1.79	0.707	1.34	2.44	0.037	6.864
28	0.016	0.12	1.93	0.757	1.38	2.5	0.041	7.356
30	0.03	0.17	2.06	0.776	1.44	2.56	0.045	7.889
32	0.045	0.23	2.13	0.784	1.47	2.61	0.048	8.307
36	0.065	0.295	2.19	0.79	1.54	2.69	0.054	8.984
38	0.074	0.31	2.21	0.791	1.58	2.72	0.056	9.295
42	0.087	0.32	2.23	0.788	1.61	2.76	0.062	9.75
46	0.097	0.327	2.23	0.783	1.62	2.81	0.068	10.065
50	0.140	0.326	2.22	0.777	1.62	2.85	0.072	10.318
55	0.109	0.319	2.21	0.768	1.61	2.86	0.074	10.51
60	0.113	0.312	2.2	0.759	1.61	2.87	0.076	10.639
65	0.115	0.305	2.19	0.747	1.6	2.87	0.077	10.704
70	0.114	0.3	2.18	0.737	1.59	2.87	0.077	10.74
75	0.112	0.297	2.16	0.728	1.58	2.86	0.076	10.732
80	0.109	0.293	2.14	0.716	1.56	2.85	0.075	10.678
90	0.104	0.28	2.07	0.695	1.52	2.81	0.07	10.416
100	0.099	0.27	2	0.67	1.48	2.77	0.065	10.104
110	0.096	0.264	1.95	0.661	1.44	2.74	0.062	9.844
120	0.093	0.257	1.9	0.652	1.41	2.71	0.059	9.601
140	0.089	0.235	1.82	0.64	1.36	2.66	0.054	9.16
160	0.085	0.206	1.76	0.621	1.32	2.59	0.048	8.729
180	0.082	0.167	1.71	0.593	1.28	2.52	0.043	8.333
200	0.081	0.119	1.68	0.563	1.24	2.44	0.038	7.965
AE (eV)	23.5±1.2	21.0±0.7	14.0±0.4	14.3±0.5	12.0±0.3eV	11.5±0.3	11.4±0.3	

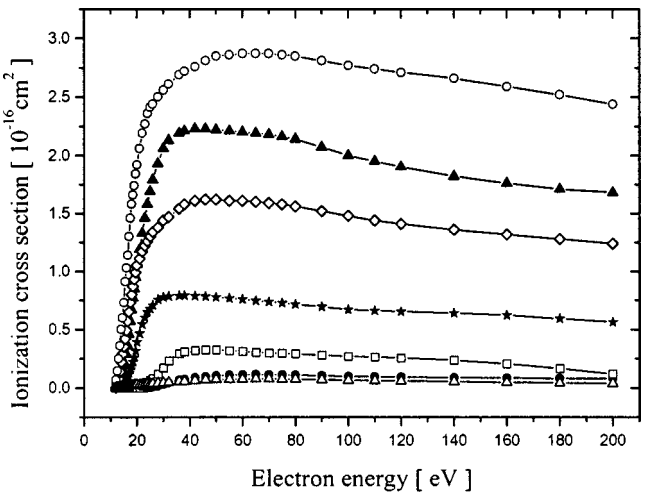

FIG. 4. Absolute partial B_2H_6 ionization cross sections for $B_2H_6^+$ (open triangles), $B_2H_5^+$ (open circles), $B_2H_4^+$ (open diamonds), $B_2H_3^+$ (closed stars), $B_2H_2^+$ (closed triangles), B_2H^+ (open squares), and B_2^+ (closed circles) as a function of electron energy up to 200 eV.

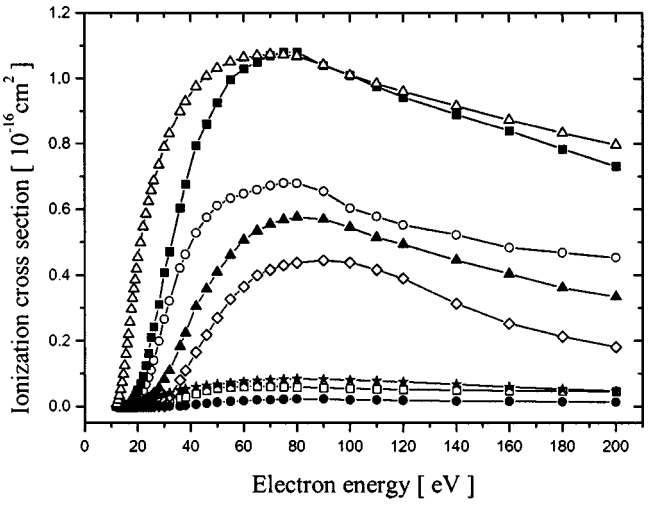

FIG. 5. Present absolute partial B_2H_6 ionization cross sections for BH_2^+ (open squares), BH_2^+ (closed squares), BH^+ (closed triangles), B^+ (open circles), H_3^+ (closed circles), H_2^+ (closed stars), H^+ (open diamonds), and absolute total B_2H_6 ionization cross section reduced by a factor of 10 (open triangles) as a function of electron energy up to 200 eV.

ionization of H-containing molecules under single collision conditions. The unusual molecular structure of B_2H_6 in conjunction with the comparatively high appearance energy of the H_3^+ ion might suggest that their formation proceeds via the initial breaking of one or both of the hydrogen bridges followed by a rearrangement and subsequent decomposition of the BH_2^+ ions that are formed in this process.

The cross-section curves of all ions show a very similar shape as a function of impact energy. The cross sections increase rapidly from threshold to a maximum and then decrease slightly with higher impact energy. The maximum for the B_2-containing ions (Fig. 4) was found to be in the range between 40 and 70 eV and at higher energies around 80 eV for the B-containing ions and H^+ (Fig. 5). The total ionization cross-section curve of diborane (last column of Table I) is shown in Fig. 5. The curve exhibits a maximum at 70 eV with a peak value of 10.74×10^{-16} cm^2. It is obvious from the cross-section curves shown in Figs. 4 and 5 that dissociative ionization is the dominant process for impact energies above 40 eV. Only the four fragment ions H_2^+, H_3^+, BH_3^+, and B_2^+ have maximum cross-section values of less than 0.1×10^{-16} cm^2, which is comparable to the maximum value of the $B_2H_6^+$ parent ionization cross section. The largest maximum cross-section values were obtained for the $B_2H_5^+$ fragment ion (2.87×10^{-16} cm^2 at 70 eV) followed by $B_2H_2^+$(2.18×10^{-16} cm^2 at 70 eV), $B_2H_4^+$(1.59×10^{-16} cm^2 at 70 eV), and BH_2^+(1.07×10^{-16} cm^2 at 70 eV). These ions account for about 72% of the total ionization cross section of B_2H_6 at 70 eV. The ion spectrum in the low energy region, which is of special interest for low-temperature plasma technology, changes with increasing impact energy due to different appearance potentials for the various ions, but is also dominated by $B_2H_5^+$, $B_2H_4^+$, and $B_2H_2^4$. For example, their contribution amounts to 88% of the total ionization cross-section value at 20 eV.

IV. CONCLUSIONS

We measured the absolute partial electron impact ionization cross sections for the B_2H_6 molecule using a time-of-flight mass spectrometric technique. The mass spectrum at 70 eV is in good agreement with known mass spectral cracking patterns of B_2H_6 for the higher ion masses. Differences with previously published data at lower ion masses can be explained in terms of the excess kinetic energy of these fragment ions, which may have affected the earlier measurements. Intensity and appearance energy values for the fragment ions H_3^+, H_2^+, and H^+ are given for the first time. A complete set of the absolute ionization cross sections for the formation of all ions from B_2H_6 was determined in the energy range from threshold to 200 eV. These results represent the first complete set of electron-impact ionization cross-section data of B_2H_6. The absolute cross-section values measured here are indispensable for a microscopic understanding and the detailed modeling of the plasma chemical processes in B_2H_6-containing plasmas. The data presented here are also important for the critical evaluation of mass spectrometric plasma diagnostics data.

ACKNOWLEDGMENT

One of the authors (K.B.) wishes to acknowledge financial support from the U.S. Department of Energy.

[1] J. L. Andujar, E. Bertran, and M. C. Polo, J. Vac. Sci. Technol. A **16**, 578 (1998).
[2] T. Iehiki and T. Yoshida, Appl. Phys. Lett. **64**, 851 (1994).
[3] B. Doris, J. Fretwell, J. L. Erskine, and S. K. Banerjee, Appl. Phys. Lett. **70**, 2819 (1997).
[4] S. Sakai, M. Takahashi, and M. Tanjyo, Rev. Sci. Instrum. **71**, 960 (2000).
[5] T. Kamiya, K. Nakahata, K. Ro, and I. Shimizu, Thin Solid Films **394**, 230 (2001).
[6] J. H. Wilson and H. A. McGee, Jr., J. Chem. Phys. **46**, 1444 (1967).
[7] W. S. Koski, J. J. Kaufmann, C. F. Pachuki, and F. J. Shipko, J. Am. Chem. Soc. **80**, 3202 (1958).
[8] J. L. Margrave, J. Chem. Phys. **61**, 38 (1957).
[9] T. P. Fehlner and W. S. Koski, J. Am. Chem. Soc. **86**, 581 (1964).
[10] A. B. Baylis, G. A. Pressley, Jr., and F. E. Stafford, J. Am. Chem. Soc. **88**, 2428 (1966).
[11] B. Ruscic, C. A. Mayhew, and J. Berkowitz, J. Chem. Phys. **88**, 5580 (1988).
[12] L. Asbrink, A. Svensson, W. Von Niessen, and G. Bieri, J. Electron. Spectrosc. Relat. Phenom. **24**, 293 (1981).
[13] D. R. Lloyd and N. Lynaugh, Philos. Trans. R. Soc. London, Ser. A **268**, 97 (1970).
[14] C. R. Brundle, M. B. Robin, H. Basch, M. Pinsky, and A. Bond, J. Am. Chem. Soc. **92**, 3836 (1970).
[15] T. Rose, R. Frey, and B. Brehm, J. Chem. Soc. D: Chem. Commun. **1969**, 1518; Erratum, **1970**, 460.
[16] NIST Database (webbook.nist.gov/chemistry/form-ser.html)
[17] V. Tarnovsky, A. Levin, K. Becker, R. Basner, and M. Schmidt, Int. J. Mass Spectrom. Ion Processes **133**, 175 (1994).
[18] R. Basner, M. Schmidt, V. Tarnovsky, A. Levin, and K. Becker, J. Chem. Phys. **103**, 211 (1995).
[19] R. Basner, R. Foest, M. Schmidt, F. Sigeneger, P. Kurunczi, K. Becker, and H. Deutsch, Int. J. Mass Spectrom. Ion Processes **153**, 65 (1996).
[20] R. Basner M. Schmidt, V. Tarnovsky, K. Becker, and H. Deutsch, Int. J. Mass Spectrom. Ion Processes **171**, 83 (1997).
[21] R. Basner, R. Foest, M. Schmidt, K. Becker, and H. Deutsch, Int. J. Mass. Spectrom. **176**, 245 (1998).
[22] R. Basner, M. Schmidt, K. Becker, V. Tarnovsky, and H. Deutsch, Thin Solid Films **374**, 291 (2000).
[23] R. Basner, M. Schmidt, E. Denisov, K. Becker, and H. Deutsch, J. Chem. Phys. **114**, 1170 (2001).
[24] P. Basner, M. Schmidt, E. Denisov, P. Lopata, K. Becker, and H. Deutsch, Int. J. Mass. Spectrom. **214**, 365 (2002).
[25] R. Basner, M. Schmidt, K. Becker, and H. Deutsch, Bull. Am. Phys. Soc. **46**, 27 (2001).
[26] D. Rapp and J. Englander-Golden, Chem. Phys. **43**, 1464 (1965).
[27] R. Rejoub, B. G. Lindsay, and R. F. Stebbings, Phys. Rev. A **65**, 042713 (2002).
[28] N. N. Greenwood and A. Earnshaw, *Chemistry of Elements* (Butterworth/Heinemann, Oxford, 2001).
[29] *CRC Handbook of Chemistry and Physics*, edited by D. R. Lide (CRC, Boca Raton, 1999).
[30] F. W. McLafferty and F. Turecek, *Interpretation von Massenspektren* (Springer, Heidelberg, 1995).
[31] M. Schmidt, Beitr. Plasmaphys. **9**, 11 (1968).
[32] A. Canosa, J. C. Gomet, B. R. Rowe, J. B. A. Mitchell, and J. L. Queffelec, J. Chem. Phys. **97**, 1028 (1992).